International Journal of Science Engineering and Advance Technology, IJSEAT, Vol 1, Issue 5, October - 2013 | ISSN 2321-6905

International Journal of Science Engineering and Advance Technology

A PROJECT ON ANALYSIS OF BI-DIRECTIONAL DC-DC CONVERTER WITH CLOSED LOOP CONTROL

[1]I.Mahesh Babu, [2]Firozali Mohammed
PG Scholar, Associate Professor
NCET, Vijayawada
[1]maheshbabu.ikk@gmail.com, [2] firozalimd1@gmail.com

Abstract— A novel bidirectional dc–dc converter is presented in this paper. The circuit configuration of the proposed converter is very simple. The proposed converter employs a coupled inductor with same winding turns in the primary and secondary sides. In step-up mode, the primary and secondary windings of the coupled inductor are operated in parallel charge and series discharge to achieve high step-up voltage gain. In step-down mode, the primary and secondary windings of the coupled inductor are operated in series charge and parallel discharge to achieve high step-down voltage gain. Thus, the proposed converter has higher step-up and step-down voltage gains than the conventional bidirectional dc–dc boost/buck converter. Under same electric specifications for the proposed converter and the conventional bidirectional boost/buck converter, the average value of the switch current in the proposed converter is less than the conventional bidirectional boost/buck converter. The operating principle and steady-state analysis are discussed in detail. Finally, a 14/42-V prototype circuit is implemented to verify the performance for the automobile dual-battery system.

Index Terms—Bidirectional dc–dc converter, coupled inductor.

I. INTRODUCTION

BIDIRECTIONAL dc–dc converters are used to transfer the power between two dc sources in either direction. These converters are widely used in applications, such as hybrid electric vehicle energy systems [1]–[4], uninterrupted power supplies [5],[6], fuel-cell hybrid power systems [7]–[10], photovoltaic hybrid power systems [11], [12], and battery chargers [13]–[15]. Many bidirectional dc–dc converters have been researched. The bidirectional dc–dc flyback converters are more attractive due to simple structure and easy control [2], [16],[17]. However, these converters suffer from high voltage stresses on the power devices due to the leakage inductor energy of the transformer. In order to recycle the leakage inductor energy and to minimize the voltage stress on the power devices, some literatures present the energy regeneration techniques to clamp the voltage stress on the power devices and to recycle the leakage inductor energy [18], [19]. Some literatures research the isolated bidirectional dc–dc converters, which include the half-bridge [8], [9], [20], [21] and full-bridge types [13], [22]. These converters can provide high step-up and step-down. voltage gain by adjusting the turns ratio of the transformer. For non-isolated applications, the non-isolated bidirectional dc–dc converters, which include the conventional boost/buck [1], [5], [12], [14], multilevel [4],

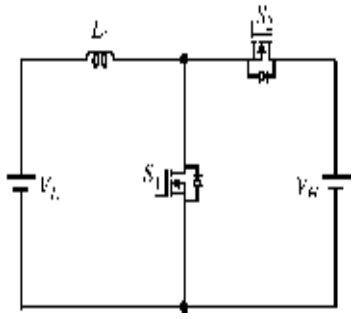

Fig. 1. Conventional bidirectional dc–dc boost/buck converter

ISSN 2321-6905

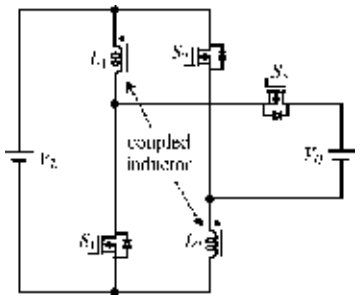

Fig. 2. Proposed bidirectional dc–dc converter.

three-level [10], sepic/zeta [23], switched capacitor [24], and coupled inductor types [25], are presented. The multilevel type is a magneticless converter, but 12 switches are used in this converter. If higher step-up and step-down voltage gains are required, more switches are needed. This control circuit becomes more complicated. In the three-level type, the voltage stress across the switches on the three-level type is only half of the conventional type. However, the step-up and step-down voltage gains are low. Since the sepic/zeta type is combined of two power stages, the conversion efficiency will be decreased. The switched capacitor and coupled inductor types can provide high step-up and step down voltage gains. However, their circuit configurations are complicated. Fig. 1 shows the conventional bidirectional dc–dc boost/buck converter which is simple structure and easy control. However, the step-up and step-down voltage gains are low.

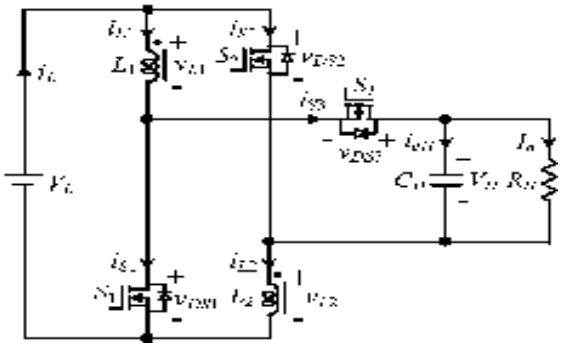

Fig. 3. Proposed converter in step-up mode.

A modified dc–dc boost converter is presented [26]. The voltage gain of this converter is higher than the conventional dc–dc boost converter. Based on this converter, a novel bidirectional dc–dc converter is proposed, as shown in Fig. 2. The proposed converter employs a coupled inductor with same winding turns in the primary and secondary sides. Comparing to the proposed converter and the conventional bidirectional boost/buck converter, the proposed converter has the following advantages: 1) Higher step-up and step-down voltage gains and 2) lower average value of the switch current under same electric specifications. The following sections will describe the operating principles and steady-state analysis for the step-up and step-down modes. In order to analyze the steady-state characteristics of the proposed converter, some conditions are assumed: The ON-state resistance RDS(ON) of the switches and the equivalent series resistances of the coupled inductor and capacitors are ignored; the capacitor is sufficiently large; and the voltages across the capacitor can be treated as constant.

II. STEP UP MODE

The proposed converter in step-up mode is shown in Fig. 3 The pulsewidth modulation (PWM) technique is used to control the switches S1 and S2 simultaneously. The switch S3 is the synchronous rectifier.

Since the primary and secondary winding turns of the coupled inductor is same, the inductance of the coupled inductor in the primary and secondary sides are expressed as

$$L_1 = L_2 = L. \quad (1)$$

Thus, the mutual inductance M of the coupled inductor is given by where k is the coupling coefficient of the coupled inductor.

$$M = k\,L_1\,L_2 = kL \quad (2)$$

The voltages across the primary and secondary windings of the coupled inductor are as follows:

$$v_{L1} = L_1 \frac{di_{L1}}{dt} + M \frac{di_{L2}}{dt} = L \frac{di_{L1}}{dt} + KL \frac{di_{L2}}{dt} \quad (3)$$

$$v_{L2} = M \frac{di_{L1}}{dt} + L_2 \frac{di_{L2}}{dt} = KL \frac{di_{L1}}{dt} + L \frac{di_{L2}}{dt} \quad (4)$$

Fig. 4 shows some typical waveforms in continuous conduction mode (CCM) and discontinuous conduction mode (DCM).

The operating principles and steady-state analysis of CCM and DCM are described as follows.

A. CCM Operation

i. *Mode 1:* During this time interval $[t_0, t_1]$, S_1 and S_2 are turned on and S_3 is turned off. The current flow path is shown in Fig. 5(a). The energy of the low-voltage side V_L is transferred to the coupled inductor. Meanwhile, the primary and secondary windings of the coupled inductor are in parallel. The energy stored in the capacitor C_H is discharged to the load. Thus, the voltages across L_1 and L_2 are obtained as

$$v_{L1} = v_{L2} = V_L \quad (5)$$

Substituting (3) and (4) into (5), yielding

$$\frac{di_{L1}(t)}{dt} = \frac{di_{L2}(t)}{dt} = \frac{VL}{(1+K)L}, \quad t0 \le t \le t1 \quad (6)$$

2) Mode 2: During this time interval $[t_1, t_2]$, S_1 and S_2 are turned off and S_3 is turned on. The current flow path is shown in Fig. 5(b). The low-voltage side V_L and the coupled inductor are in series to transfer their energies to the capacitor C_H and the load. Meanwhile, the primary and secondary windings of the coupled inductor are in series. Thus, the following equations are found to be

$$i_{L1} = i_{L2} \quad (7)$$

$$v_{L1} + v_{L2} = V_L - V_H. \quad (8)$$

Substituting (3), (4), and (7) into (8), yielding

$$\frac{di_{L1}(t)}{dt} = \frac{di_{L2}(t)}{dt} = \frac{VL - V_H}{2(1+K)L}, \quad t1 \le t \le t2 \quad (9)$$

By using the state-space averaging method, the following equation is derived from (6) and (9):

$$\frac{DV_L}{(1+K)L} + \frac{(1-D)(V_L - V_H)}{2(1+K)L} = 0 \quad (10)$$

Simplifying (10), the voltage gain is given

$$G_{CCM(step\_up)} = \frac{V_H}{V_L} = \frac{(1+D)}{1-D} \quad (11)$$

B. DCM Operation

1) Mode 1: During this time interval $[t_0, t_1]$, S_1 and S_2 are turned on and S_3 is turned off. The current flow path is shown in Fig. 5(a). The operating principle is same as that for the mode 1 of CCM operation. From (6), the two peak currents through the primary and secondary windings of the coupled inductor are given by

$$I_{L1p} = I_{L2p} = \frac{V_L D T_S}{(1-K)L} \quad (12)$$

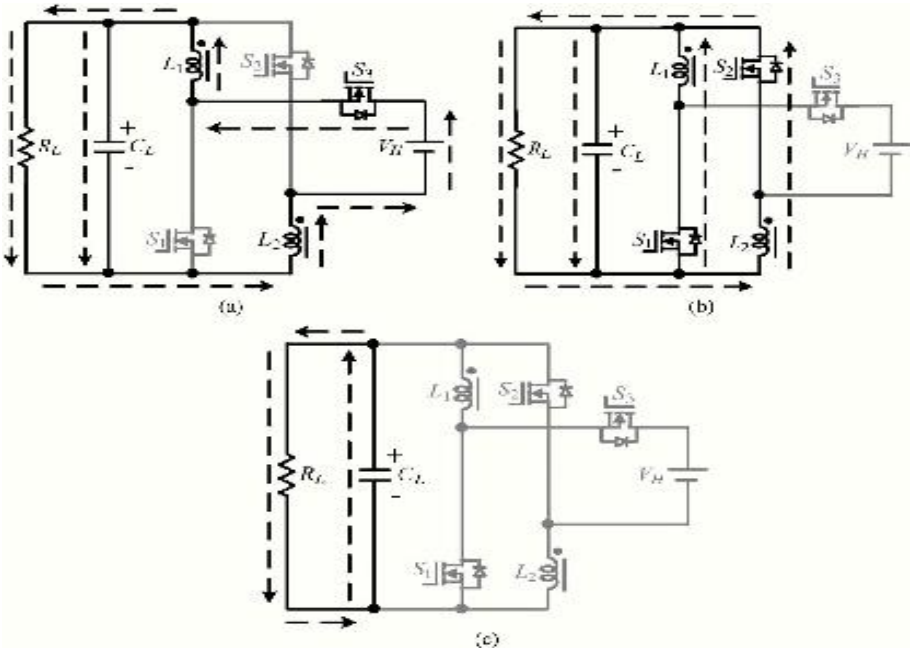

Fig.3. Current ow path of the proposed converter in step-down mode. (a) Mode 1. (b) Mode 2. (c) Mode 3 for DCM operation

Mode 2: During this time interval [t_1, t_2], S_1 and S_2 are turned off and S_3 is turned on. The current flow path is shown in Fig. 5(b). The low-voltage side V_L and the coupled inductor are in series to transfer their energies to the capacitor C_H and the load. Meanwhile, the primary and secondary windings of the coupled inductor are in series. The currents i_{L1} and i_{L2} through the primary and secondary windings of the coupled inductor are decreased

to zero at $t = t_2$. From (9), another expression of I_{L1p} and I_{L2p} is given by

$$\mathrm{I}_{L1p} = I_{L2p} = \frac{(V_H - V_L)D_2T_S}{2(1+K)L} \quad (13)$$

Mode 3: During this time interval [t_2, t_3], S_1 and S_2 are still turned off and S_3 is still turned on. The current flow path is shown in Fig. 5(c). The energy stored in the coupled inductor is zero. Thus, i_{L1} and i_{L2} are equal to zero. The energy stored in the capacitor C_H is discharged to the load.

From (12) and (13), D_2 is derived as follows :

$$D_2 = \frac{2DV_L}{VH - VL} \quad (14)$$

From Fig. 4(b), the average value of the output capacitor current during each switching period is given by

$$\mathrm{I_{cH}} = \frac{\frac{1}{2}\mathrm{D_2T_sI_{L1p}} - \mathrm{I_0T_s}}{\mathrm{T_s}} = \frac{1}{2}\mathrm{D_2I_{L1p}} - \mathrm{I_0} \quad (15)$$

Substituting (12) and (14) into (15), I_{cH} is derived as

$$I_{cH} = \frac{D^2 V_L{}^2 T_S}{(1+K)L(V_H - V_L)} - \frac{V_H}{R_H} \quad (16)$$

Since I_{cH} is equal to zero under steady state, (16) can be

rewritten as follows:

$$\frac{D^2 V_L{}^2 T_S}{(1+K)L(V_H - V_L)} = \frac{V_H}{R_H} \quad (17)$$

Then, the normalized inductor time constant is defined as

$$\tau_{LH} = \frac{L}{R_H T_S} = \frac{L f_S}{R_H} \quad (18)$$

where f_s is the switching frequency. Substituting (18) into (17), the voltage gain is given by

$$G_{DCM(step-up)} = \frac{V_H}{V_L} = \frac{1}{2} + \sqrt{\frac{1}{4} + \frac{D^2}{(1+K)\tau_{LH}}} \quad (19)$$

C. Boundary Operating Condition of CCM and DCM

When the proposed converter in step-up mode is operated in boundary conduction mode (BCM), the voltage gain of CCM operation is equal to the voltage gain of DCM operation. From (11) and (19), the boundary normalized inductor time constant $\tau_{LH,B}$ can be derived as follows:

$$\tau_{LH,B} = \frac{D(1-D)^2}{2(1+K)(1+D)} \quad (20)$$

The curve of $\tau_{LH,B}$ is plotted in Fig. 6. If τ_{LH} is larger than $\tau_{LH,B,}$ the proposed converter in step-up mode is operated in CCM.

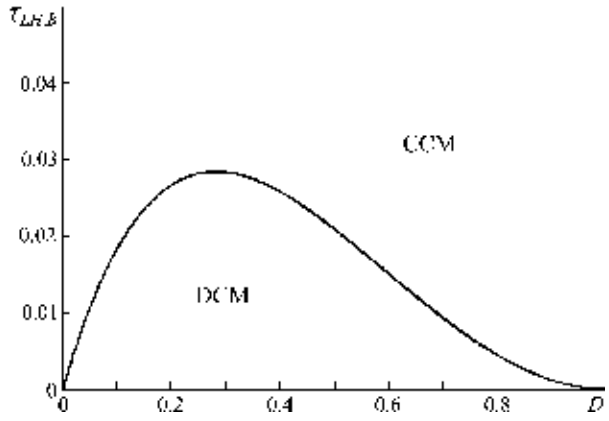

Fig. 6. Boundary condition of the proposed converter in step-up mode(assuming k =1).

3) Mode 3: During this time interval [t_2, t_3], S_1 and S_2 are still turned off and S_3 is still turned on. The current flow path is shown in Fig. 5(c). The energy stored in the coupled inductor is zero. Thus, i_{L1} and i_{L2} are equal to zero. The energy stored in the capacitor C_H is discharged to the load.

From (12) and (13), D_2 is derived as follows:

$$D_2 = \frac{2DV_L}{VH - VL} \quad (14)$$

From Fig. 4(b), the average value of the output capacitor current during each switching period is given by

$$I_{cH} = \frac{\frac{1}{2} D_2 T_S I_{L1p} - I_0 T_S}{T_S} = \frac{1}{2} D_2 I_{L1p} - I_0 \quad (15)$$

Substituting (12) and (14) into (15), I_{cH} is derived as

$$I_{cH} = \frac{D^2 V_L{}^2 T_S}{(1+K)L(V_H - V_L)} - \frac{V_H}{R_H} \quad (16)$$

Since I_{cH} is equal to zero under steady state, (16) can be

rewritten as follows:

$$\frac{D^2 V_L^2 T_S}{(1+K)L(V_H - V_L)} = \frac{V_H}{R_H} \quad (17)$$

Then, the normalized inductor time constant is defined as

$$\tau_{LH} = \frac{L}{R_H T_S} = \frac{L f_S}{R_H} \quad (18)$$

where f_s is the switching frequency. Substituting (18) into (17), the voltage gain is given by

$$GDCM(step-up) = \frac{V_H}{V_L} = \frac{1}{2} + \sqrt{\frac{1}{4} + \frac{D^2}{(1+K)\tau_{LH}}} \quad (19)$$

B. Boundary Operating Condition of CCM and DCM

When the proposed converter in step-up mode is operated in boundary conduction mode (BCM), the voltage gain of CCM operation is equal to the voltage gain of DCM operation. From (11) and (19), the boundary normalized inductor time constant $\tau_{LH,B}$ can be derived as follows:

$$\tau_{LH,B} = \frac{D(1-D)^2}{2(1+K)(1+D)} \quad (20)$$

The curve of $\tau_{LH,B}$ is plotted in Fig. 6. If τ_{LH} is larger than $\tau_{LH,B,}$ the proposed converter in step-up mode is operated in CCM.

I. STEP-DOWN MODE

Fig. 7 shows the proposed converter in step-down mode. The PWM technique is used to control the switch S_3. The switches S_1 and S_2 are the synchronous rectifiers. Fig. 8 shows some typical waveforms in CCM and DCM. The operating principle and steady-state analysis of CCM and DCM are described as follows Fig. 6. Boundary condition of the proposed converter in step-up mode (assuming k =1).

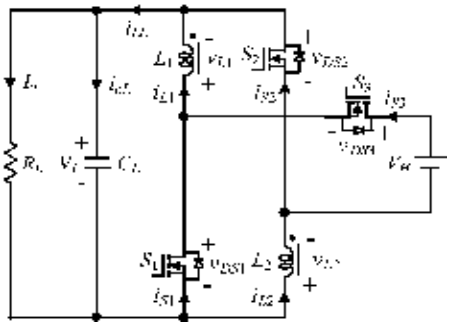

Fig. 7. Proposed converter in step-down mode.

A. CCM Operation

1) *Mode 1:* During this time interval [t_0, t_1], S_3 is turned on and S_1/S_2 are turned off. The current flow path is shown in Fig. 9(a). The energy of the high-voltage side V_H is transferred to the coupled inductor, the capacitor C_L, and the load. Meanwhile, the primary and secondary windings of the coupled inductor are in series. Thus, the following equations are given as:

Substituting (3), (4), and (21) into (22), yielding

$$\frac{di_{L1}(t)}{dt} = \frac{di_{L2}(t)}{dt} = \frac{V_L - V_H}{2(1+K)L}, \quad t0 \le t \le t1 \quad (23)$$

$$i_{L1} = i_{L2} \quad (21)$$

$$v_{L1} + v_{L2} = V_H - V_L \quad . (22$$

I. EXPERIMENTAL RESULTS

In order to verify the performance of the proposed converter, a 14/42-V prototype circuit is built in the laboratory for the automobile dual-battery system. The electric specifications and circuit components are selected as VL = 14 V, VH = 42 V, fs = 50 kHz, Po = 200 W, CL = CH = 330 μF, $L1$ = $L2$ =15.5 μH ($rL1$ = $rL2$ = 11 mΩ). Also, MOSFET IRF3710 ($VDSS$ = 100 V, $RDS(ON)$ = 23 mΩ, and ID = 57 A) is selected for $S1$, $S2$, and $S3$.Some experimental results in step-up and step-down modes are shown in Figs. 18–21. Fig. 18(a) shows the waveforms of the input current iL and the coupled inductor currents $iL1$ and $iL2$ in step-up mode. It can be seen that $iL1$ is equal to $iL2$. The

current *iL* is double of the level of the coupled-inductor current during *S*1/*S*2 ON-period and equals the coupled-inductor current during *S*1/*S*2 OFF-period. Fig. 20(a) shows the waveforms of the current *iLL* and the coupled-inductor currents *iL*1 and *iL*2 in step-down mode. It can be observed that *iL*1 is equal to *iL*2. The current *iLL* equals to the coupled-inductor current during *S*3 ON-period and is double of the level of the coupled-inductor current during *S*3 OFF-period. Figs. 18(b) and 20(b) show the waveforms of the switch current *iS*1, *iS*2, and *iS*3 in step-up and stepdown modes, respectively. As can be seen in Figs. 18(c) and 20(c), the voltage stresses on *S*1 and *S*2 equal (*VH* + *VL*)/2. Also, the voltage stress on *S*3 equals *VH* + *VL*. Figs. 19 and 21 show the dynamic response of the proposed converter in step-up and step-down modes. One can see that the output voltage is well regulated.

Fig. 18. Some experimental waveforms of the proposed converter in step-up mode. (a) iL1 , iL2 ,andiL ,(b)iS 1 , iS 2 ,andiS 3 .(c)vDS 1 , vDS 2 ,andvD S3 .

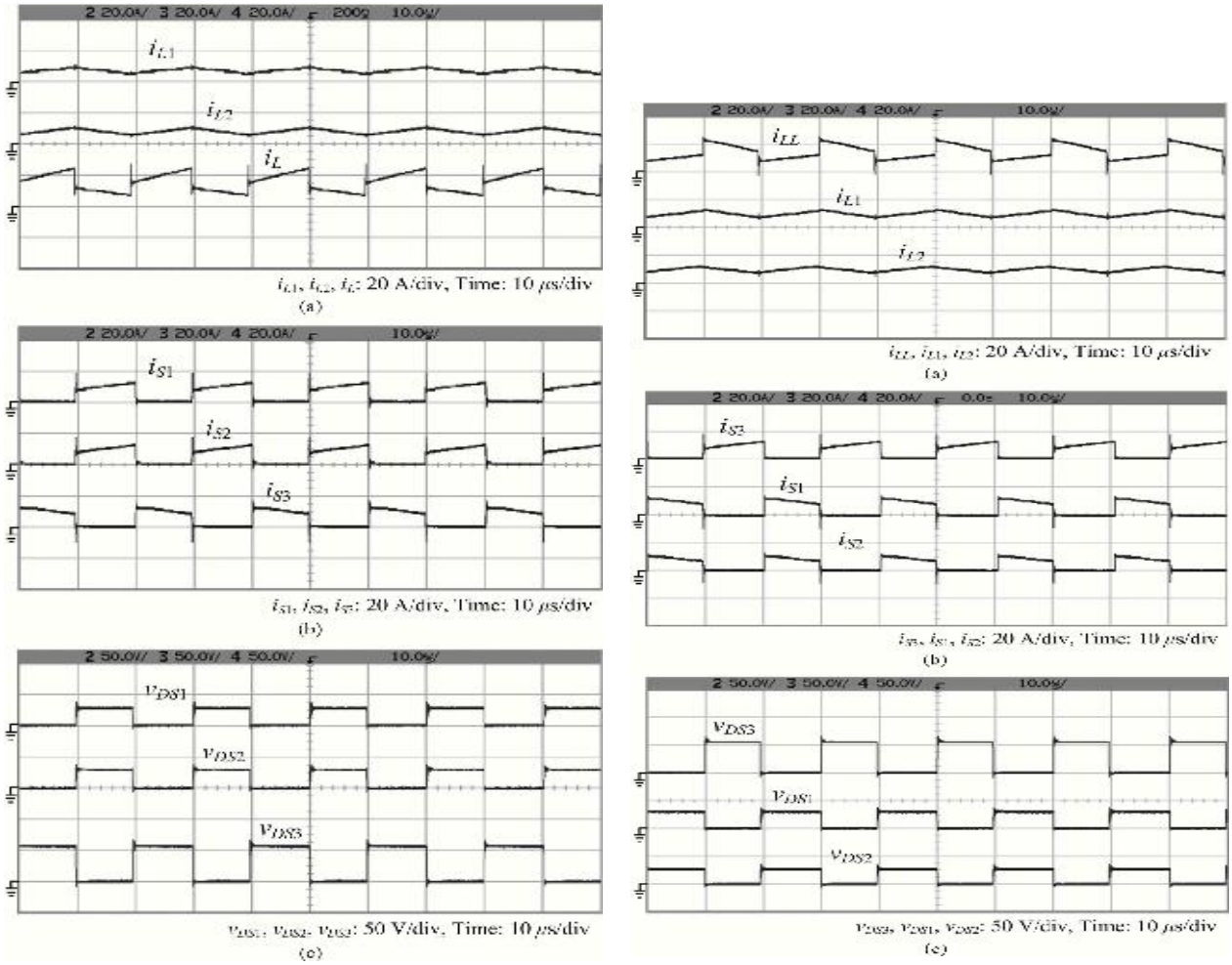

Fig. 19. Dynamic response of the proposed converter in step-up mode for the output power variation between 20 and 200 W.

Moreover, the prototype circuit of the conventional bidirectional boost/buck converter is also implemented in the laboratory. The electric specifications and circuit components are selected as VL = 14V, VH = 42V, fs = 50kHz, Po = 200 W,$L1$ = 28 μH ($rL1$ = 15 mΩ), CL = CH = 330 μF. Also, MOSFET IRF3710 is selected for $S1$ and $S2$. The measured efficiency in the proposed converter and the conventional bidirectional boost/buck converter are shown in Fig. 22. At full-load condition, the measured efficiency of the proposed converter is 92.7% in step-up mode and is 93.7% in step-down mode. Also, the measured efficiency of the proposed converter is around 92.7%–96.2% in step-up mode and is around 93.7%–96.7% in step-down mode. Also, it is seen from Fig. 22 that the measured efficiency of the proposed converter are higher than the conventional bidirectional boost/buck converter.

I. CONCLUSION

This paper researches a novel bidirectional dc–dc converter.

The circuit configuration of the proposed converter is very simple. The proposed converter has higher step-up and step-down voltage gains and lower average value of the switch current than the conventional bidirectional boost/buck converter. From the experimental results, it is see that the experimental waveforms agree with the operating principle and steady-state analysis. At full-load condition, the measured efficiency is 92.7% in stepup mode and is 93.7% in step-down mode. Also, the measured efficiency is around 92.7%–96.2% in step-up mode and is around 93.7%–96.7% in step-down mode, which are higher than the conventional bidirectional boost/buck converter.

REFERENCES

[1] M. B. Camara, H. Gualous, F. Gustin, A. Berthon, and B. Dakyo, "DC/DC converter design for super capacitor and battery power management in hybrid vehicle applications—Polynomial control strategy," *IEEE Trans. Ind. Electron.*, vol. 57, no. 2, pp. 587–597, Feb. 2010.

[2] T. Bhattacharya, V. S. Giri, K. Mathew, and L. Umanand, "Multiphase bidirectional flyback converter topology for hybrid electric vehicles," *IEEE Trans. Ind. Electron.*, vol. 56, no. 1, pp. 78–84, Jan. 2009.

[3] Z. Amjadi and S. S. Williamson, "A novel control technique for a switched-capacitor-converter-based hybrid electric vehicle energy storage system," *IEEE Trans. Ind. Electron.*, vol. 57, no. 3, pp. 926–934, Mar. 2010.

[4] F. Z. Peng, F. Zhang, and Z. Qian, "A magnetic-less dc–dc converter for dual-voltage automotive systems," *IEEE Trans. Ind. Appl.*, vol. 39, no. 2, pp. 511–518, Mar./Apr. 2003.

[5] A. Nasiri, Z. Nie, S. B. Bekiarov, and A. Emadi, "An on-line UPS system with power factor correction and electric isolation using BIFRED converter," *IEEE Trans. Ind. Electron.*, vol. 55, no. 2, pp. 722–730, Feb. 2008.

[6] L. Schuch, C. Rech, H. L. Hey, H. A. Grundling, H. Pinheiro, and J. R. Pinheiro, "Analysis and design of a new high-efficiency bidirectional integrated ZVT PWM converter for DC-bus and battery-bank interface," *IEEE Trans. Ind. Appl.*, vol. 42, no. 5, pp. 1321–1332, Sep./Oct. 2006.

[7] X. Zhu, X. Li, G. Shen, and D. Xu, "Design of the dynamic power compensation for PEMFC distributed power system," *IEEE Trans. Ind. Electron.*, vol. 57, no. 6, pp. 1935–1944, Jun. 2010.

[8] G. Ma, W. Qu, G. Yu, Y. Liu, N. Liang, and W. Li, "A zero-voltageswitching bidirectional dc–dc converter with state analysis and softswitching-oriented design consideration," *IEEE Trans. Ind. electron.*, vol. 56, no. 6, pp. 2174–2184, Jun. 2009.

[9] F. Z. Peng, H. Li, G. J. Su, and J. S. Lawler, "A new ZVS bidirectional dc–dc converter for fuel cell and battery application," *IEEE Trans. Power Electron.*, vol. 19, no. 1, pp. 54–65, Jan. 2004.

[10] K. Jin, M. Yang, X. Ruan, and M. Xu, "Three-level bidirectional converter for fuel-cell/battery

hybrid power system," *IEEE Trans. Ind. Electron.*, vol. 57, no. 6, pp. 1976–1986, Jun. 2010.

[11] R. Gules, J. D. P. Pacheco, H. L. Hey, and J. Imhoff, "A maximum power point tracking system with parallel connection for PV stand-alone applications," *IEEE Trans. Ind. Electron.*, vol. 55, no. 7, pp. 2674–2683,Jul. 2008.

[12] Z. Liao and X. Ruan, "A novel power management control strategy for stand-alone photovoltaic power system," in *Proc. IEEE IPEMC*, 2009,pp. 445–449.

[13] S. Inoue and H. Akagi, "A bidirectional dc–dc converter for an energy storage system with galvanic isolation," *IEEE Trans. Power Electron.*, vol. 22, no. 6, pp. 2299–2306, Nov. 2007.

[14] L. R. Chen, N. Y. Chu, C. S. Wang, and R. H. Liang, "Design of a reflex based bidirectional converter with the energy recovery function," *IEEE Trans. Ind. Electron.*, vol. 55, no. 8, pp. 3022–3029, Aug. 2008.

[15] S. Y. Lee, G. Pfaelzer, and J. D.Wyk, "Comparison of different designs of a 42-V/14-V dc/dc converter regarding losses and thermal aspects," *IEEE Trans. Ind. Appl.*, vol. 43, no. 2, pp. 520–530, Mar./Apr. 2007.

[16] K. Venkatesan, "Current mode controlled bidirectional flyback converter," in *Proc. IEEE Power Electron. Spec. Conf.*, 1989, pp. 835–842.

[17] T. Qian and B. Lehman, "Coupled input-series and output-parallel dual interleaved flyback converter for high input voltage application," *IEEE Trans. Power Electron.*, vol. 23, no. 1, pp. 88–95, Jan. 2008.

[18] G. Chen, Y. S. Lee, S. Y. R. Hui, D. Xu, and Y. Wang, "Actively clamped bidirectional flyback converter," *IEEE Trans. Ind. Electron.*, vol. 47, no. 4, pp. 770–779, Aug. 2000.

[19] F. Zhang and Y. Yan, "Novel forward-flyback hybrid bidirectional dc–dc converter," *IEEE Trans. Ind. Electron.*, vol. 56, no. 5, pp. 1578–1584, May2009.

I.Mahesh Babu Pursuing M.Tech in Nimra College of Engineering and Technology, Vijayawada .His specialization is Power & Industrial Drives. He graduated in Electrical and Electronics Engineering from Dr.Paulraj Engineering college JNTUH. (maheshbabu.ikk@gmail.com)

Firozali Mohammed is currently working as a Associate Professor in Electrical and Electronics Engineering Department, Nimra College of Engineering and Technology (NCET), Vijayawada. He obtained his M.Tech Degree in Power Electronics from Sathyabama University, Chennai. He received B.Tech degree in Electrical and Electronics Engineering from NCET, Vijayawada. His research interest includes Power Electronic Converters and applications. (firozalimd1@gmail.com)